Segmented Stator Switched Reluctance Motor Drive for Light Electric Vehicle

Pere Andrada*, Balduí Blanqué, Marcel Torrent, Pol Kobeaga
GAECE, Department of Electrical Engineering, EPSEVG
UPC BARCELONA-TECH
Av. Víctor Balaguer 1, 08800 Vilanova i la Geltrú, Spain
Email: pere.andrada@upc.edu
* *Corresponding author*

Abstract: **The world market of electric light vehicles will significantly increase in the coming years. What will require the development of better high-performance drives with low-cost, and, if possible, free of permanent magnets. A segmented stator switched reluctance motor is presented to fulfill this objective because it has advantages over the conventional switched reluctance machines, such as segmented stator construction, stator shorter flux paths without flux reversal, and as a consequence, fewer iron losses. Simulations will demonstrate that the proposed segmented stator switched reluctance motor drive is suitable as a powertrain for light electric vehicles.**

Keywords: **Finite element analysis, light electric vehicles, modular stator, switched reluctance machines.**

I. INTRODUCTION

The electric light vehicles world market will increase notably in the coming years. To drive this growth, it is necessary to develop drives with high torque to weight ratio, more efficient, and low cost. Currently, manufacturers of electric vehicles are trying to reduce or even suppress permanent magnets in the powertrain of electric vehicles. The Switched Reluctance Motor (SRM) is a good choice among permanent magnet-free motors, although it has worst features than permanent magnet synchronous motors, such as lower power density, higher torque ripple, and higher acoustic noise. There are two ways to increase the performance of SRMs: first, to use better magnetic materials, and second to use segmented structures in the stator or the rotor. The segmented stator switched reluctance motor (SSSRM) was first proposed by Hendershot [1-4]. Later, some authors published interesting contributions about this kind of electric machine [5-10]. The SSSRM, compared to conventional SRM has the following advantages: modular or segmented stator construction, shorter flux paths without flux reversal in the stator, and then fewer iron losses. The main drawback of SSSRMs over conventional SRMs is the reduction of space for the coils of the windings due to the particular arrangement of stator U-shaped cores. The principal objective of this work is to prove if SSSRM drives are suited as a powertrain, with mechanical transmission, for the propulsion of light electric vehicles (LEVs), including losses assessment. This paper is organized as follows: after the introduction, the basic principles of SSSRM are explained in section 2. In section 3, a description of the SSSRM drive for the propulsion of LEVs is given. Section 4 is about the finite element analysis of the proposed SSSRM. Section 5 presents losses evaluation in SSSRMs. Simulations of the whole SSSRM drive, considering the machine, the electronic power converter, and the control strategies, are exposed in section 6. At last, in section 7, conclusions from this investigation are presented.

II. FUNDAMENTALS OF SSSRM

The SSSRM, with m phases, is composed by N_U independent U-shaped stator cores, and N_R rotor poles with the angles shown in Fig. 1.

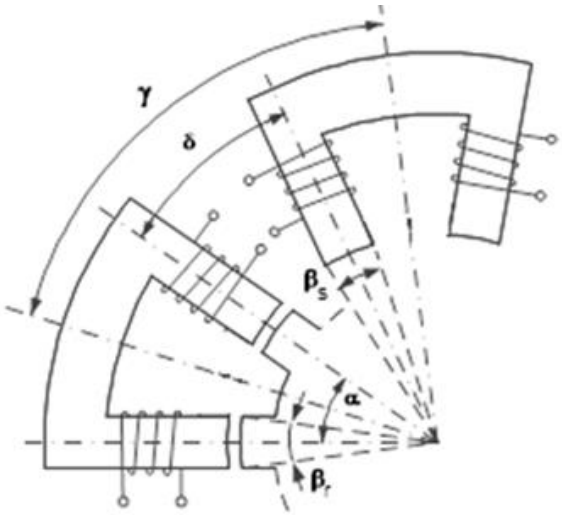

Fig. 1. Geometrical disposition of the SSSRM.

An m-phase SSSRM must fulfill the following relationships:

$$N_U = k\ m \tag{1}$$

Being k, multiplicity (No. of working stator pole pairs).

The No. of stator poles, *Ns*, is equal to:

$$N_S = 2\ k\ m \tag{2}$$

And the No. rotor poles, N_R:

$$N_R = k\,(2m - 1) \tag{3}$$

The angle between the axes of two consecutive U-shaped cores, γ, is given by:

$$\gamma = \frac{360^0}{N_U} \tag{4}$$

The angle between the rotor poles, α, is equal to:

$$\alpha = \frac{360^0}{N_R} \tag{5}$$

And the angle between the axes of stator poles of the two consecutive U-shaped cores, δ, is:

$$\delta = \gamma - \alpha = \frac{360^0\,(N_R - N_U}{N_U\,N_R} \tag{6}$$

The stator pole angle, β_S, should accomplish:

$$\beta_S < \frac{\alpha}{2} \tag{7}$$

The rotor pole angle, β_R, should be slightly larger than the stator pole angle, that is:

$$\beta_R > \beta_S \tag{8}$$

III. DESCRIPTION OF THE PROPOSED DRIVE

An electric drive for the propulsion of a LEV with the torque on the wheel-speed characteristics of Fig. 2 has to be designed. Between motor and wheel, there is a chain and sprocket drive with a transmission ratio of 4.57 (64/14) and an efficiency of 98%. Therefore, the torque-angular velocity characteristic of the SSSRM drive must be that shown in Fig. 3. In this characteristic, there are two important points: point A, the maximum angular velocity at which the maximum torque is maintained (1396 r/min; 27.90 Nm) and point B, the maximum angular velocity at which the maximum power is maintained (4063 r/min; 9.59 Nm), therefore between points A and B, the power is constant (4 kW).

For this purpose, a three-phase SSSRM with multiplicity 2 has been selected, being the stator formed by 6 independent U-core with 12 stator poles while the rotor has 10 poles. In each U-shaped core, there are two coils wound on each of their legs and connected in series. The parallel connection of the diametrically opposite U-shaped core coils forms a motor phase. The conductors are of a rectangular section to ease winding manufacture, increase fill factor and improve heat dissipation. Fig. 4 shows a cross-section of the proposed 12-10 SSSRM prototype, designed following the procedure explained in [11], and table I gives its main data. The SSSRM will be powered from an electronic power controller specially designed for SRM that is widely described in [12].

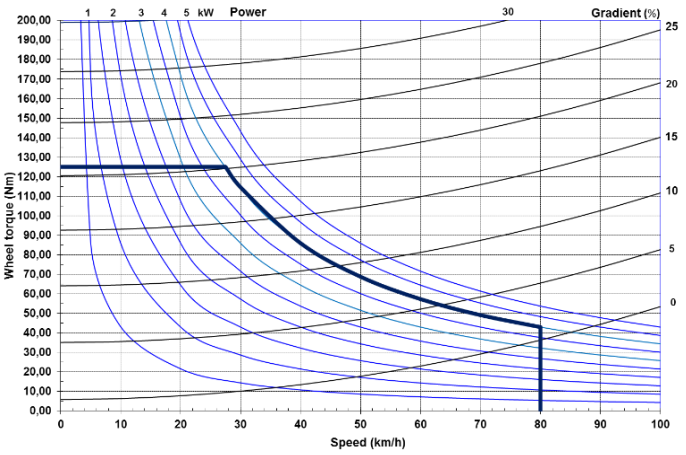

Fig. 2. Torque on the wheel vs speed and gradient characteristic of the LEV.

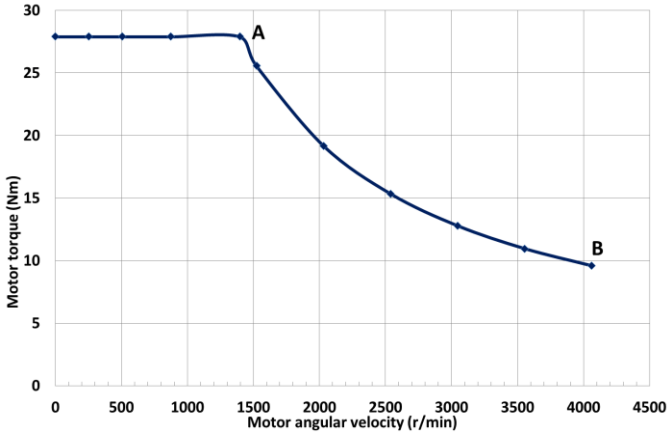

Fig. 3. Torque vs motor angular velocity characteristic of the SSSRM drive.

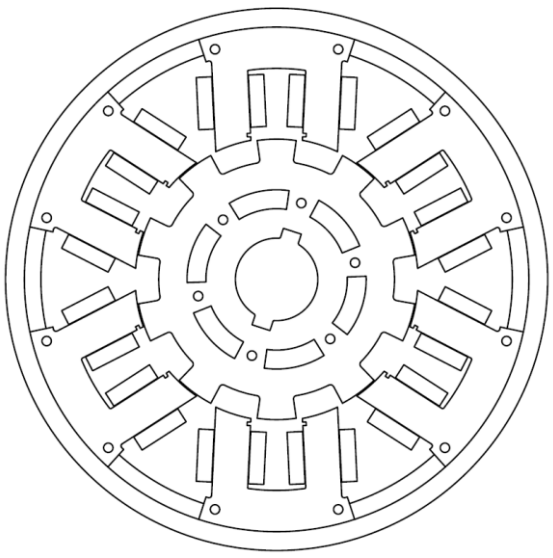

Fig. 4. Cross-section of the proposed SSSRM.

TABLE I. MAIN DATA OF THE PROTOTYPE.

Parameter	Value
U, Voltage (V)	72
m, No. of phases	3
N_U, No. of stator U shaped cores	6
N_s, No. of stator poles	12
N_R , No. of rotor poles	10
D_O, Output stator diameter (mm)	214
L, stator axial length (mm)	60
D_r , Rotor diameter (mm)	119
g, Air-gap (mm)	0.5
β_S, Stator polar angle (º)	15
β_R, Rotor polar angle (º)	16
w_S, Stator polar width (mm)	15.66
w_R, Rotor polar width (mm)	18.62
h_S, Stator yoke height (mm)	20.95
Lamination	M250-50 A (stator & rotor)
D_e, Shaft diameter (mm)	35
N_p, No. of turns per pole	10
n_p, No. of coils per phase	4
N_f, No. of turns per phase	40 (series connection)
S_c , Wire section (mm)	2 wires, each one 2x2.4 (rectangular section)
Thermal class of isolation	180ºC

IV. FINITE ELEMENT ANALYSIS OF THE PROPOSED SSSRM

Once outlined the main dimensions of the proposed 12-10 SSSRM electromagnetic finite element analysis is performed using the well-known Flux package [13]. First, the 2D finite element analysis is carried out, obtaining the magnetization curves, flux-linkage vs. current for different positions, Fig. 5, and the static torque curves vs. position for distinct values of current that are shown in Fig. 6. In Fig. 7 can be seen the map of magnetic flux density for a displacement of 9º from the unaligned position and a flat top current of 150 A; in these conditions, the torque achieves a value of 25 Nm. It is important to point out that in these simulations, 0º corresponds to the unaligned position.

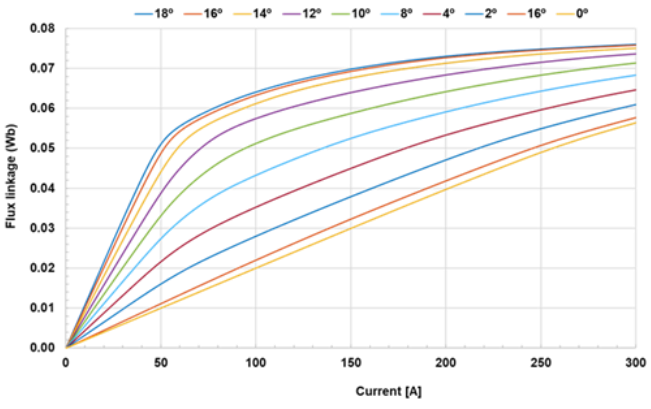

Fig. 5. 2D magnetization curves of the proposed SSSRM.

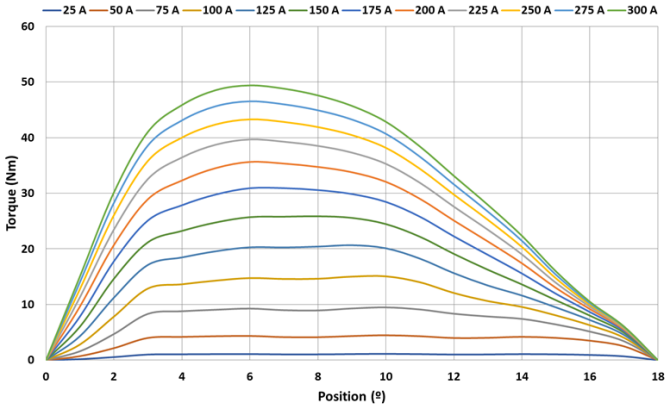

Fig. 6. 2D static torque curves of the proposed SSSRM.

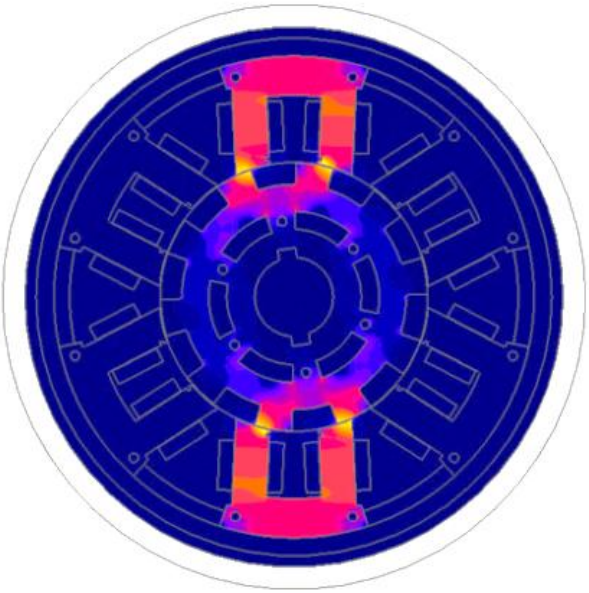

Fig.7. 2D magnetic density flux map at 9º from alignment and 150 A of the proposed SSSRM.

Then 3D finite element analysis is performed to take into account the end effects in the proposed SSSRM. Fig. 8 shows a comparison in 2D and 3D between the magnetization curves in aligned and unaligned positions. In Fig. 9, some static torque curves vs. position in 2D and 3D are compared. The discrepancy in the magnetization curves in 2D and 3D is large at unaligned position and especially at high values of current. In contrast, the results are in the right concordance in the aligned position. The static torque differences in 2D and 3D are lower but increase with higher current values. Fig. 10 shows the magnetic density flux map in 3D in the same conditions as the analysis in 2D.

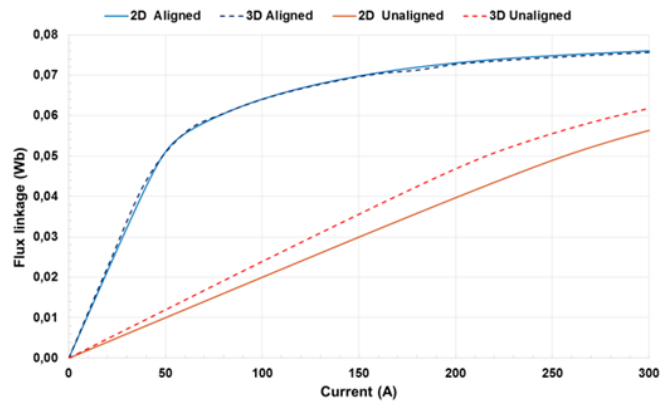

Fig. 8. Comparison of 2D and 3D magnetization curves of the proposed SSSRM.

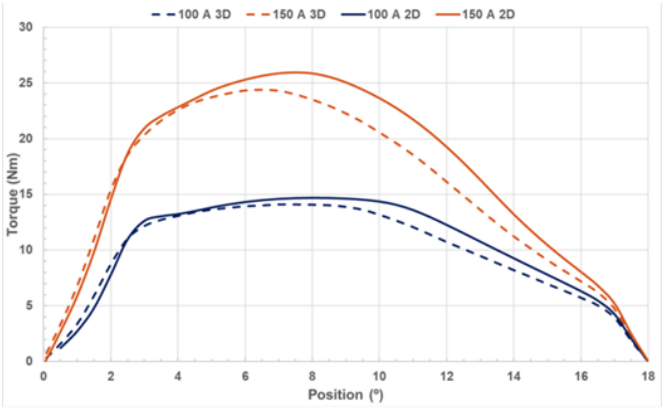

Fig. 9. Comparison of static torque curves in 2D and 3D of the proposed SSSRM.

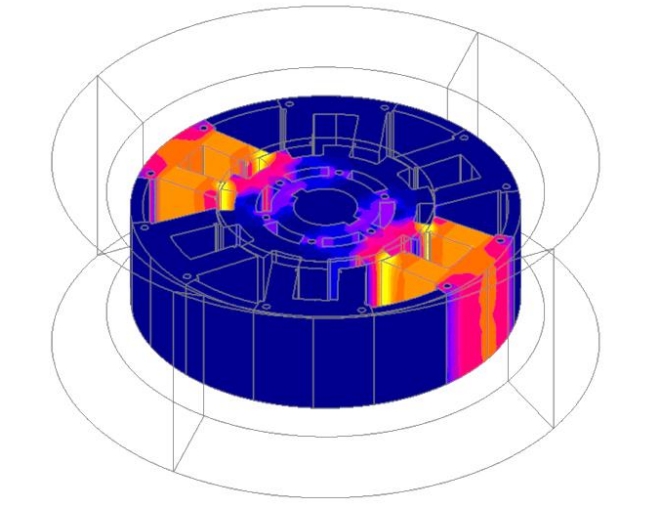

Fig.10. 3D magnetic density flux map at 9º from alignment and 150 A of the proposed SSSRM.

V. ASSESSMENT OF LOSSES IN THE SSSRM

The copper losses at temperature θ are calculated by:

$$p_{cu\theta} = \rho_{20º} \frac{235+\theta}{255} \frac{N_f l_{em}}{S_c} k_s I_f^2 \quad (9)$$

With:

ρ_{20^o}, Copper resistivity at 20ºC (Ωmm²/m)
N_f, No. of turns per phase
l_{em}, length of average turn (m)
S_c, conductor section (mm²)
k_s, skin factor.
I_f, RMS value of phase current (A).

The mechanical losses are estimated by the following empirical equation:

$$p_{mec} = k_{fb} G N \cdot 10^{-3} + 2 D_r^3 L N^3 \cdot 10^{-6} \quad (10)$$

With:

k_{fb}, constant (in this case 3)
G, mass of rotor (kg)
D_r, outer diameter of the rotor (m)
N, angular velocity (r/min)
L, length of core (m).

The specific iron losses (W/kg) in the different parts that must be considered are the combination of hysteresis, eddy current and excess losses. In the case of SSSRM, these parts (i) are the stator U shaped core, the rotor poles, and the rotor yoke according to:

$$p_{espFe\,(i)} = k_h f_i^{\alpha} B_i^{\beta} + k_e f_i^2 B_i^2 + k_{ex} f_i^{\frac{3}{2}} B_i^{\frac{3}{2}} \quad (11)$$

Where f is the frequency, see table II, and B the peak magnetic flux density in each of the different parts considered computed by finite elements according to the current required by the operating conditions. The values of α, β, k_h, k_e and k_{ex} for the used lamination M250-50A are obtained from [14]. The total iron losses are determined by:

$$p_{iron} = \sum_{i=1}^{n} (p_{espFe\,(i)} G_i) \quad (12)$$

With G_i mass of the different parts considered.

TABLE II. FREQUENCY AT DIFFERENT PARTS OF THE SSSRM.

	Stator U shaped core	**Rotor poles and rotor yoke**
Frequency	$N_R \frac{N\,(r/\min)}{60}$ The same frequency of phase currents	$\frac{N\,(r/\min)}{60}$

VI. SIMULATION OF THE PROPOSED SSSRM DRIVE

Simulations of the drive, considering the SSSRM, the electronic power converter, an asymmetric half bridge converter (classic converter) with two switches and two diodes per phase, and the control are performed using Matlab-Simulink and some results of the finite element

analysis of the SSSRM. The Simulink model, Fig. 11, is the same used in [15] adapted to the proposed SSSRM drive. The drive operates at 72 V, using hysteresis control with variable turn-on (ϑ_{ON}) and turn-off (ϑ_{OFF}) angles at low-medium angular velocity, and single pulse control with variable turn-on (ϑ_{ON}) and turn-off (ϑ_{OFF}) angles at high angular velocity. The phase voltage, total torque phase current, flux, and DC bus current waveforms are plotted in Fig. 12 for an average torque of 28.98 Nm at 1400 r/min with ϑ_{ON} = - 2º, and ϑ_{OFF} = 15º being the current reference 175 A and the phase (RMS) current of 114.94 A. In Fig. 13 the same waveforms are shown for an average torque of 12.72 Nm at 3500 r/min with ϑ_{ON} = -5º and ϑ_{OFF} = 13º with a current reference of 100 A and the phase (RMS) current of 66.69 A. It should be noted that ϑ_{ON} and ϑ_{OFF} angles are referenced to the non-aligned position (0º). In Fig. 14, the expected envelope of torque-angular velocity of the SSSRM drive (blue-line) is compared with the simulation results (black rhombic markers). Also, in this figure, the values of efficiency vs. angular velocity are shown at the simulated points (red-line). These results demonstrate the suitability of SSSRM drive for the propulsion of the proposed LEV.

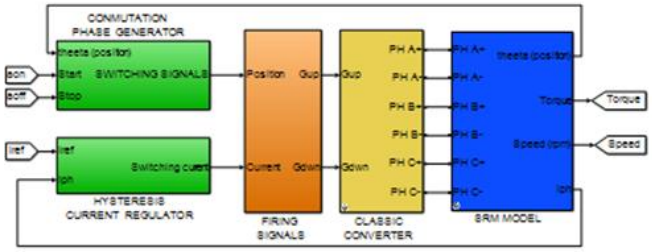

(a)

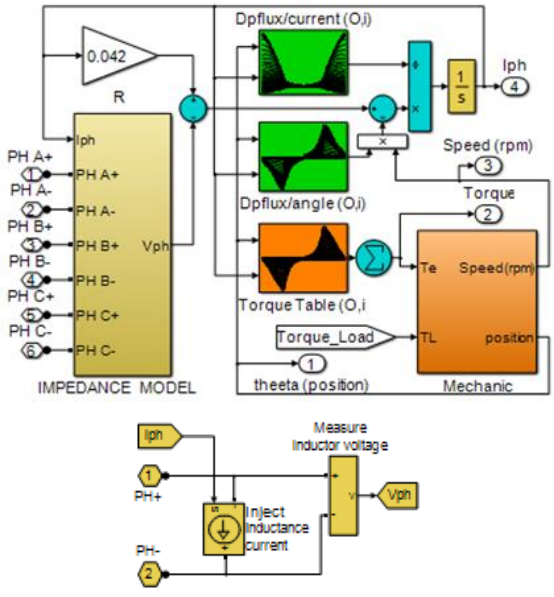

(b)

Fig. 11. (a) Block diagram of the complete SSSRM drive. (b) Detailed Matlab- Simulink model of the SSSRM.

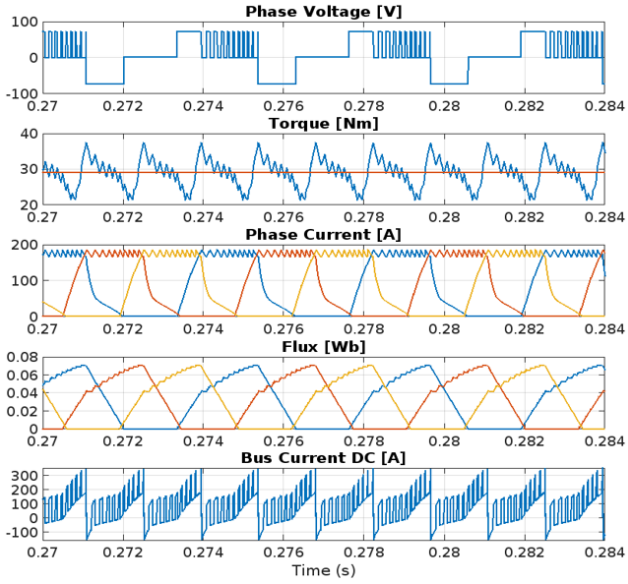

Fig. 12. Waveforms for an average torque of 28.98 Nm at 1400 r/min.

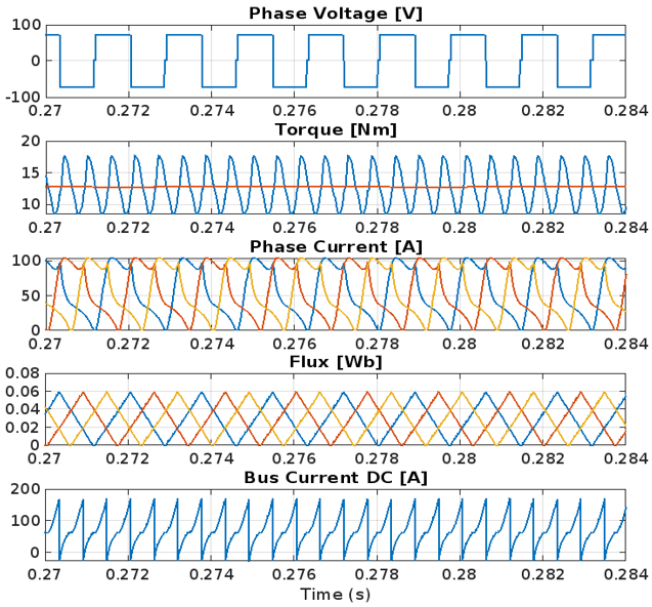

Fig. 13. Waveforms for an average torque of 12.72 Nm at 3500 r/min.

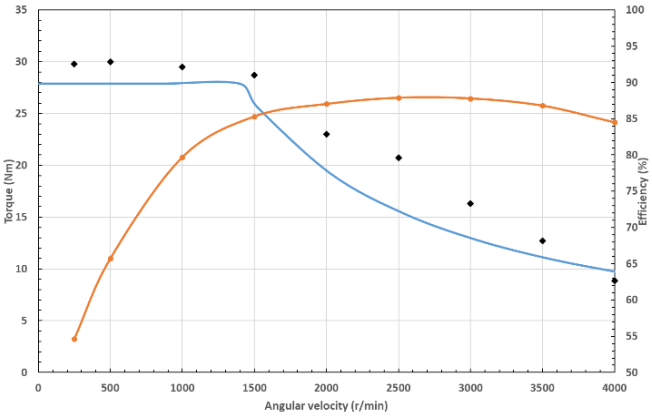

Fig. 14. Comparative between the expected values of the of torque-angular velocity envelope (blue line) with the simulated values (black rhombic markers) and simulated efficiency-angular velocity curve (red line).

VII. CONCLUSIONS

A segmented stator switched reluctance motor drive for the propulsion of LEVs with specified torque-angular velocity characteristics has been presented. This SSSRM is a three-phase, with 6 U-shaped cores, 12 stator poles, and 10 rotor poles. 2D and 3D electromagnetic finite element analyses are performed, as well as an evaluation of the motor losses. The simulation of the complete drive, considering the motor, the power converter, and different control strategies, is implemented in Matlab-Simulink using some results obtained from the electromagnetic analysis. Simulations have demonstrated that the features of the proposed SSSRM drive are suitable for the propulsion of LEVs.

ACKNOWLEDGMENT

This work was supported by the project TED 2021-129912B-I00.

REFERENCES

[1] J. R. Hendershot. “Short flux paths cool SR motors,” *Machine Design*, September 1989, pp.106-111.
[2] J. R. Hendershot. “Switched reluctance brushless DC motors with low loss magnetic circuits,” *Proceedings Intelligent Motion*, October 1989.
[3] J. R. Hendershot. “Polyphase electronically commutated reluctance motor,” US Patent 4883999, 1989.
[4] C. Hancock and J. R. Hendershot. “Electronically commutated reluctance motor,” US Patent 5015903, 1991.
[5] M. T. Khor and R. Sotudeh. “A 3-Phase 12/10 asymmetrical switched reluctance motor,” *EPE 2005*, Dresden. DOI: 10.1109/EPE.2005.219463.
[6] T. Burress and C. Ayers. “Development and experimental characterization of a multiple isolated flux path reluctance machine,” *2012 IEEE Energy Conversion Congress and Exposition*, pp. 899-905. DOI: 10.1109/ECCE.2012.6342723.
[7] R. Jaeger, S. S. Nielsen, P. O. Rasmussen and K. Kongerslev. “Development and analysis of U-core switched reluctance machine,” *2016 IEEE Energy Conversion Congress and Exposition (ECCE)*. DOI: 10.1109/ECCE.2016.7855037.
[8] S. R. Mousavi-Aghdam, M. Reza Feyzi, N. Bianchi and M. Morandin, “Design and analysis of a novel high torque stator-segmented SRM,” *IEEE Transactions on Industrial Electronics*, vol. 63, pp. 1458-1466, 2016. DOI: 10.1109/TIE.2015.2494531.
[9] M. Terzic, B. Brkovic and D. Mihic. “Dynamic model of segmented stator switched reluctance motor with bypass coils,” *2020 International Conference on Electrical Machines (ICEM 2020)*, pp. 687-693. DOI: 10.1109/ICEM49940.2020.9270937.
[10] Design of a three-phase switched reluctance motor with 12 stator poles and 10 rotor poles for an electric motorcycle. (in Spanish): Diseño de un motor de reluctancia autoconmutado (SRM) trifásico con 12 polos en el estator y 10 polos en el rotor para una motocicleta eléctrica. Luis Lara, TFG EPSEVG directed by P. Andrada, October 2017.
[11] P. Andrada. “Design of a segmented switched reluctance drive for a light electric vehicle”. *Renewable energy and power quality journal*, 1 September 2022, vol. 20, p. 662-667.DOI:10.24084/repqj20.394
[12] P. Andrada, B. Blanqué, M. Capó, G. Gross and D. Montesinos. “Switched Reluctance Motor Controller for Light Electric Vehicles,” *20th European Conference on Power Electronics and Applications (EPE'18 ECCE Europe)*, 2018, pp. 1-11.
[13] Flux 12.1, Altair: Troy, MI, USA, 2021.
[14] N. Fernando and F. Hanin. “Magnetic materials for electrical machine design and future research directions: a review,” *2017 IEEE International Electric Machines and Drives Conference (IEMDC)*, DOI: 10.1109/IEMDC.2017.8002412.
[15] P. Andrada, E. Martínez, B. Blanqué, M. Torrent, J. I. Perat and J. A. Sánchez. “New axial-flux switched reluctance motor for e-scooter,” *ESARS ITEC*, Toulouse, 2-4 November 2016. DOI: 10.1109/ESARS-ITEC.2016.7841417.